PERGAMON

International Journal of Heat and Mass Transfer 44 (2001) 799–810

International Journal of HEAT and MASS TRANSFER

www.elsevier.com/locate/ijhmt

Similarity simulation for Marangoni convection around a vapor bubble during nucleation and growth

David M. Christopher*, Bu-Xuan Wang

Thermal Engineering Department, Tsinghua University, Beijing 100084, China

Received 20 March 2000

Abstract

Marangoni convection occurs around vapor bubbles during nucleation and growth due to the temperature variation along the surface. The surface tension variation resulting from the temperature gradient along the surface causes Marangoni convection. Marangoni convection is of importance in crystal growth melts and may influence other processes with liquid–vapor interfaces, in addition to boiling. The influence of Marangoni induced convection is more obvious under microgravity but also occurs in earth gravity. This paper presents a similarity solution for Marangoni induced flow both for the velocity profile and the temperature profile, assuming developing boundary-layer flow along a surface with various imposed temperature profiles. The surface velocity, the total flow rate and the heat transfer characteristics are given for various temperature profiles and various Prandtl numbers. Since the predicted boundary layer thickness would be much less than the diameter of vapor bubbles during nucleate boiling, the bubble surface curvature effects can be neglected and this analysis can be used as a first estimate of the effect of Marangoni flow around a vapor bubble.

Keywords: Marangoni convection; Similarity solution; Bubble movement; Nucleate boiling

1. Introduction

Marangoni convection occurs around vapor bubbles during nucleation and the growth of vapor bubbles due to the surface tension variation caused by temperature and/or concentration variations along the bubble surface. Experimental tests and numerical analyses of nucleate boiling have shown that the heat transfer due to Marangoni flow can be significant under microgravity and may also be important in earth gravity [1,2]. Marangoni induced flow is also of importance in crystal growth melts where the flow produces undesirable effects under microgravity in the same manner as buoyancy induced natural convection [3].

Numerous investigations of Marangoni convection have been reviewed in the literature, for example by Arafune and Hirata [4] and Croll et al. [5] Some papers very relevant to this work include the order-of-magnitude analysis of Marangoni induced flow given by Okano et al. [6] showing the general trends for the Grashof number, Marangoni number, Prandtl number and melt aspect ratio on the Reynolds number. Some experimental and numerical investigations of Marangoni flow for various substances in geometries with flat surfaces were presented by Arafune and Hirata [4], Okano et al. [6], and Arafune et al. [7]. Very recently,

* Corresponding author. Tel.: +86-10-62772986; fax: +86-10-62770209.

E-mail address: dmc@tsinghua.edu.cn (D.M. Christopher).

0017-9310/01/$ - see front matter
PII: S0017-9310(00)00129-0

Nomenclature

a, d, h	exponents in similarity transformation
A	temperature gradient coefficient (K/m^{k+1})
C_1	similarity transformation coefficient (m^a)
C_2	similarity transformation coefficient ($s\ m^{(k-4)/3}$)
$f(\eta)$	stream function similarity variable
K	temperature gradient exponent
$\dot{m}$	mass flow rate per unit width (kg/m s)
m	correlation coefficient in Eq. (31)
n	correlation coefficient in Eq. (31)
Ma	Marangoni number, Eq. (17)
Nu	Nusselt number, Eq. (22)
Pr	Prandtl number
q''	heat flux (W/m^2)
Re	Reynolds number, Eq. (18)
T	temperature (K)
u, v	velocities (m/s)
x, y	coordinates (m)

Greek symbols

α	thermal diffusivity (m^2/s)
δ	boundary layer thickness (m)
ϕ	dimensionless similarity temperature
η	location similarity variable
η_δ	dimensionless momentum boundary layer thickness
η_t	dimensionless thermal boundary layer thickness
λ	thermal conductivity (W/m K)
μ	dynamic viscosity ($N\ s/m^2$)
ν	kinematic viscosity (m^2/s)
θ	temperature similarity variable ($K\ m^h$)
ρ	density (kg/m^3)
σ	surface tension (N/m)
ψ	stream function (m^2/s)

Subscripts

L	average over surface length
x	local value
t	thermal boundary layer thickness
δ	momentum boundary layer thickness

Arafune and Hirata [8] presented a similarity analysis for the velocity profile for thermal and solutal Marangoni flow, but the results are effectively limited to surface tension variations linearly related to the surface position. Slavtchev and Miladinova [9] presented similarity solutions for surface tension that varied as a quadratic function of the temperature as would occur near a minimum. Schwabe and Metzger [10] experimentally investigated the Marangoni convection on a flat surface combined with natural convection in a unique geometry where the Marangoni effect and the buoyancy effect could be varied independently.

This paper presents a similarity solution for Marangoni induced flow over a flat surface due to an imposed temperature gradient. The analysis assumes that the surface tension varies linearly with temperature but the temperature variation is a power-law function of the location. In addition, the analysis assumes that a boundary layer develops along the surface due to the coupled Marangoni convection. The boundary layer equations for both the momentum equations and the energy equation are transformed to ordinary differential equations which are then solved numerically using the Runge–Kutta method.

2. Theoretical analysis

For laminar boundary layer flow over a flat plate, the Navier–Stokes equations can be reduced to the continuity equation and the boundary layer momentum (Eq. (8)):

$$\frac{\partial u}{\partial x}+\frac{\partial v}{\partial y}=0 \tag{1}$$

$$u\frac{\partial u}{\partial x}+v\frac{\partial u}{\partial y}=\upsilon\frac{\partial^2 u}{\partial y^2} \tag{2}$$

The boundary layer energy equation is:

$$u\frac{\partial T}{\partial x}+v\frac{\partial T}{\partial y}=\alpha\frac{\partial^2 T}{\partial y^2} \tag{3}$$

The Marangoni effect is incorporated as a boundary condition relating the temperature field to the velocity field. The boundary conditions at the surface are:

$$\mu\left.\frac{\partial u}{\partial y}\right|_{y=0}=-\frac{\mathrm{d}\sigma}{\mathrm{d}T}\left.\frac{\partial T}{\partial x}\right|_{y=0} \tag{4a}$$

$$v(x,0)=0 \tag{4b}$$

$$T(x,0)=T(0,0)+Ax^{k+1} \tag{4c}$$

Far from the surface, the velocity boundary condition is:

$$u(x,\infty)=0 \tag{5a}$$

Two thermal boundary conditions can be considered:

$$T(x,\infty)=T_\infty=\ T(0,0)\quad\text{or}\quad \left.\frac{\partial T}{\partial y}\right|_{y=\infty}=0 \tag{5b}$$

For the stream function defined as:

$$u=\frac{\partial\psi}{\partial y}\quad\text{and}\quad v=-\frac{\partial\psi}{\partial x} \tag{6}$$

similarity variables can be introduced as:

$$\eta=C_1x^d y \tag{7a}$$

$$f(\eta)=C_2x^a\psi(x,y) \tag{7b}$$

$$\theta(\eta)=(T(x,y)-T(0,0))x^h \tag{7c}$$

and then the governing equations can be written as:

$$f'''=f'^{\,2}(d-a)+a\,ff'' \tag{8a}$$

$$\theta''=Pr(a\,f\theta'-h\,f'\theta) \tag{8b}$$

where the coefficients are defined as:

$$C_1=\sqrt[3]{\frac{(\mathrm{d}\sigma/\mathrm{d}T)A\rho}{\mu^2}} \tag{9a}$$

$$C_2=\sqrt[3]{\frac{\rho^2}{(\mathrm{d}\sigma/\mathrm{d}T)A\mu}} \tag{9b}$$

For similarity, the exponents are related to the temperature gradient exponent, k in equation Eq. (4c) by:

$$d=\frac{k-1}{3} \tag{10a}$$

$$a=\frac{-2-k}{3} \tag{10b}$$

$$h=-1-k \tag{10c}$$

The momentum equation boundary conditions are:

$$f(0)=0 \tag{11a}$$

$$f''(0)=-1 \tag{11b}$$

$$f'(\infty)=0 \tag{11c}$$

For the energy equation boundary conditions, two types of boundary conditions can be considered for the boundary condition far from the surface:

$$\theta(0)=A \tag{12a}$$

$$\theta(\infty)=0\quad\text{or}\quad\theta'(\infty)=0 \tag{12b}$$

Since the energy equation is linear, the functional representation for the temperature can be simplified by defining:

$$\theta(\eta)=A\phi(\eta) \tag{13}$$

Substituting Eq. (13) into the energy equation, Eq. (8b), and the boundary conditions, Eq. (12), gives the following equations for ϕ:

$$\phi''=Pr(a\,f\phi'-h\,f'\phi) \tag{14}$$

$$\phi(0)=1 \tag{15a}$$

$$\phi(\infty)=0\quad\text{or}\quad\phi'(\infty)=0 \tag{15b}$$

The surface velocity is given by:

$$u(x,0)=\sqrt[3]{\frac{[(\mathrm{d}\sigma/\mathrm{d}T)A]^2}{\rho\mu}}\,f'(0)x^{(2k+1)/3} \tag{16}$$

Note that the temperature gradient coefficient can be defined in terms of the total temperature difference along a surface of length, L, as $A=\Delta T/L^{k+1}$ so that the Marangoni number can be defined for a general temperature profile as:

$$Ma_L=\frac{(\mathrm{d}\sigma/\mathrm{d}T)(\Delta T/L^{k+1})L^{k+2}}{\mu\alpha}=\frac{(\mathrm{d}\sigma/\mathrm{d}T)\Delta T\,L}{\mu\alpha} \tag{17}$$

The Reynolds number, defined in terms of the surface velocity, is then related to the Marangoni number as:

$$Re_L=\frac{u(x,0)L}{\nu}\ =f'(0)\ Ma_L^{2/3}\ Pr^{-2/3} \tag{18}$$

The total mass flow in the boundary layer per unit width can be written as:

$$\dot{m}=\int_0^\infty\rho u\,\mathrm{d}y=\sqrt[3]{\frac{\mathrm{d}\sigma}{\mathrm{d}T}\,A\rho\mu}\,x^{(k+2)/3}f(\infty) \tag{19}$$

or in dimensionless form as:

$$Re_x=\frac{\rho\bar{u}\delta}{\mu}=f(\infty)Ma_x^{1/3}\ Pr^{-1/3} \tag{20}$$

The local heat flux is:

$$q''(x)=-\lambda\left.\frac{\partial T}{\partial y}\right|_{y=0}=-\lambda C_1A\phi'(0)x^{(4k+2)/3} \tag{21}$$

The local Nusselt number is:

$$Nu_x = \frac{q''(x)x}{\lambda(T(x,0) - T(x,\infty))}$$

$$= -Ma_x^{1/3}\, Pr^{-1/3}\left(\frac{x}{L}\right)^{(k+2)/3} \phi'(0) \tag{22}$$

The average Nusselt number based on the average temperature difference between the temperature of the surface and the temperature far from the surface is:

$$Nu_L = -\frac{3k+6}{4k+5}\, Ma_L^{1/3}\, Pr^{-1/3}\, \phi'(0) \tag{23}$$

The similarity transformation used here for the momentum equation differs in several ways from that used by Arafune and Hirata [8]. Besides slightly different definitions of the similarity variables, the most important difference lies in that the present derivation is based on a general form of the temperature variation on the surface. The results from Arafune and Hirata [8] are useful only for a linear variation of the surface tension with location. The present derivation is also extended to include the energy equation.

3. Similarity results with discussion

The two governing equations, Eqs. (8a) and (14), were solved numerically using the fourth-order Runge–Kutta method with at least 20 000 steps. The shooting method was used to determine the unknown boundary conditions at $\eta = 0$, i.e. $f'(0)$ for the momentum equation and $\phi'(0)$ for the energy equation. The maximum value for the independent variable, η, which was a function of the Prandtl number, was always chosen to be at least four times the maximum boundary layer thickness. The minimum value that could be used for the momentum equation was $\eta = 20$ which was sufficient for the energy equation with Prandtl numbers greater than 2. The thermal boundary layer thickness, and hence, the maximum value of η will be much greater for Prandtl numbers less than 2. The results presented here were all independent of the number of steps and the maximum value of η.

The similarity stream function, f, is a function of the exponent, k, while the temperature function, ϕ, is a function of both k and the Prandtl number. The governing equations, Eqs. (8a) and (14), were solved together with the boundary conditions in Eqs. (11), (15a) and (15b) for various values of k and Prandtl number. Typical velocity and temperature profiles are given in Fig. 1 for several representative values of Prandtl number and for $k = 0$ which is a linear surface temperature profile. The results for the two different energy equation boundary conditions at the outer edge were the same since the slopes of the temperature profiles shown in Fig. 1 (which were calculated using the boundary condition $\phi(\infty) = 0$) all approach zero at large η. When using the boundary condition $\phi'(\infty) = 0$, the value of ϕ always approached zero for large η. The magnitude of the slope of the temperature profile at

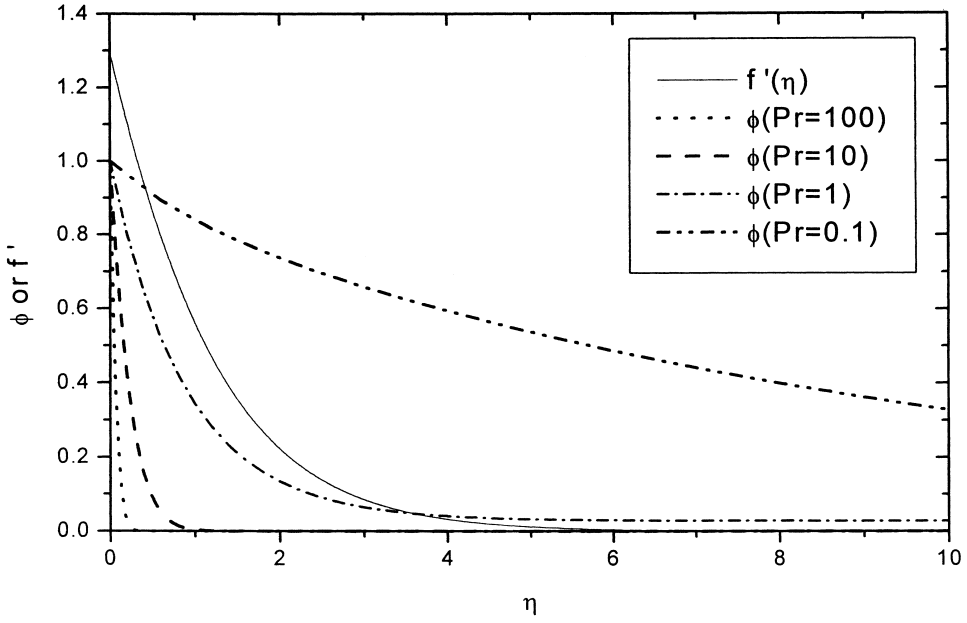

Fig. 1. Velocity and temperature profiles for $k = 0$.

the surface decreases with decreasing Prandtl number as the thermal boundary layer gets very thick for low Prandtl numbers.

The variations of the surface velocity, the boundary layer thickness and the total flow rate in the boundary layer are given as functions of k in Fig. 2, of which $k = 0$ refers to a linear profile, $k = 1$ is quadratic, while $k = -0.5$ would be a temperature variation relative to the square root of x. The minimum value of k is -1, which results in no temperature variation on the bubble surface and thus no Marangoni induced flow. The momentum boundary layer thickness was defined as usual as the point where the velocity is 1% of the surface velocity. The velocity for small values of k is greater because for a fixed total temperature difference across the surface (i.e. fixed temperature gradient coefficient, A), the surface temperature profile for a small value of k is steeper near the leading edge which provides more flow (Fig. 3). For larger values of k, the slope of the temperature profile is steeper near the trailing edge where the boundary layer is thicker and the additional acceleration of the flow has less effect. The mass flow rate, which is proportional to $f(\infty)$ in Eq. (19), follows the same trend. The boundary layer thickness is the greatest for the uniformly increasing temperature profile, $k = 0$. For k greater than or less than 0, the temperature profile over part of the plate is relatively flat, so the flow does not accelerate much in that region and the boundary layer does not grow. The boundary layer thickness, which varies from about 4 to 5 for the range in Fig. 2 and is 4.79 for the linear temperature profile, can also be used to calculate the boundary layer thickness on a curved surface such as a vapor bubble if the thickness is small compared to the curvature. For water near the normal boiling point around a bubble roughly 1 mm in diameter, the maximum boundary layer thickness is about one tenth of the bubble diameter, so the results presented here could be used at least as an initial estimate of the flow and heat transfer in the liquid boundary layer around the bubble due to Marangoni convection around the bubble.

The surface velocities are compared to the velocities measured by Arafune and Hirata [8] for gallium and indium in a shallow pool in Fig. 4. Although they measured surface velocities for other fluids (silicone oils with high Prandtl numbers), the present similarity analysis only applies to the results for the liquid metals which would essentially have a linear temperature distribution on the surface due to the high conduction heat transfer rate. The similarity results agree well with the measured velocities for indium. The similarity and experimental results both agree with the analysis of Okano et al. [6] which showed that the Reynolds number is proportional to the two-thirds power of the temperature difference. The measured velocities for gallium do not agree as well with the analysis and do not vary as the two-thirds power of the temperature perhaps due to buoyancy effects and the effect of the entire recirculating flow field in the pool.

Two typical temperature profiles for $k = 0$ and low Prandtl numbers are shown in Fig. 5. The similarity

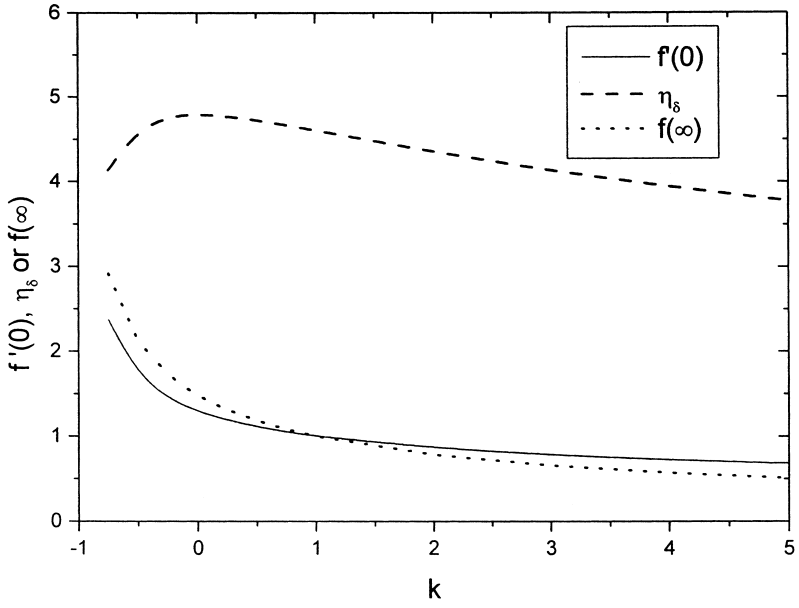

Fig. 2. Surface velocity, boundary layer thickness and flow rate for various temperature gradient exponents.

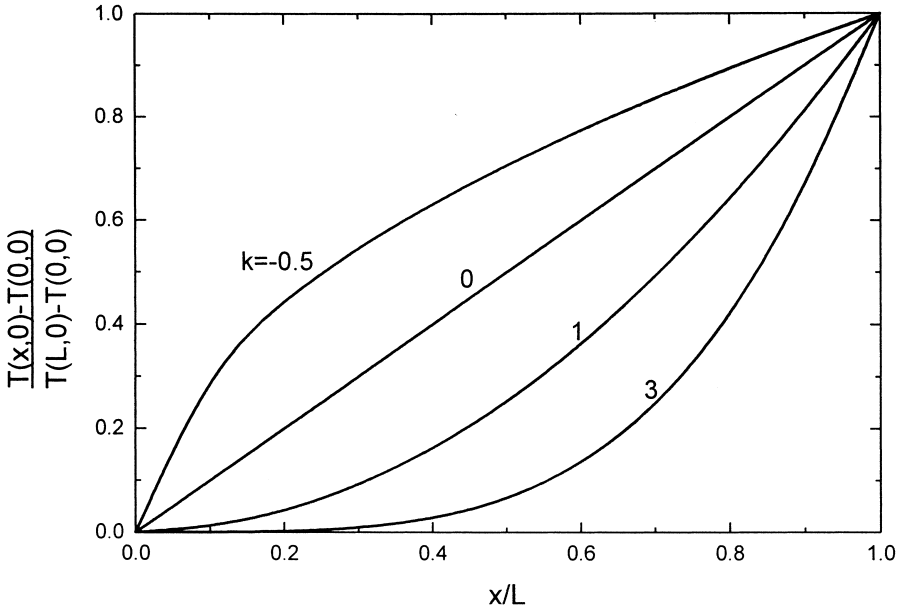

Fig. 3. Typical surface temperature profiles.

results are compared with an approximate analysis of the energy equation for low Prandtl numbers which have thermal boundary layers much thicker than the momentum boundary layers. Therefore, over most of the domain, $f'(\eta)$ is equal to zero and $f(\eta)$ is equal to $f(\infty)$ so the energy equation given in Eq. (14) can be approximated by

$$\phi'' = Pr\, a f(\infty)\phi' \tag{25}$$

The solution of Eq. (25) subject to the boundary conditions as given in Eqs. (15a) and (15b) is:

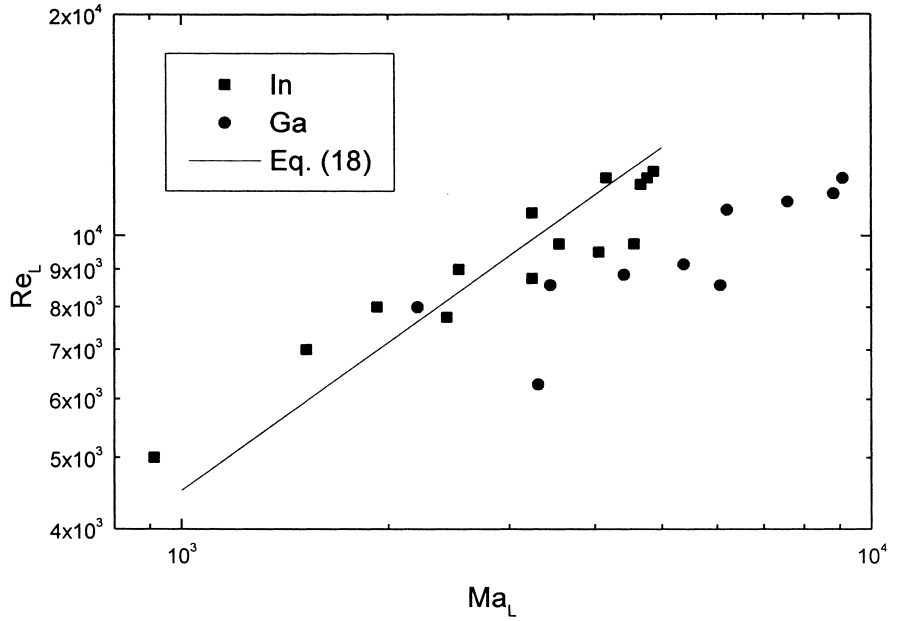

Fig. 4. Comparison of experimental results of Arafune et al. [8] with similarity result for $k = 0$ and Prandtl number for indium.

$$\phi(\eta) = e^{-Pr[(k+2)/3]f(\infty)\eta} \tag{26}$$

which is compared to the similarity solution in Fig. 5. The temperature gradient at the surface for low Prandtl numbers would then vary as

$$\phi'(0) = -Pr\left(\frac{k+2}{3}\right)f(\infty) \tag{27}$$

Therefore, the surface temperature gradient could be expected to be proportional to the Prandtl number for a given surface temperature variation and low Prandtl numbers.

For high Prandtl numbers ($Pr > 10$), the thermal boundary layer thickness is much thinner than the momentum boundary layer thickness, so the energy equation can be approximated by assuming that $f(\eta)$ is essentially zero and that $f'(\eta)$ is essentially $f'(0)$ for small η. Therefore, for high Prandtl numbers, the energy equation may be approximated by

$$\phi'' = Pr(k+1)f'(0)\phi \tag{28}$$

which has the solution

$$\phi(\eta) = e^{-\sqrt{Pr(k+1)f'(0)}\,\eta} \tag{29}$$

Then, the surface temperature gradient could be approximated by:

$$\phi'(0) = -\sqrt{Pr(k+1)f'(0)} \tag{30}$$

The variation of the surface temperature gradient as a function of the Prandtl number and the temperature gradient exponent is shown in Fig. 6. The similarity results are compared to an equation with correlation coefficients m and n of the form:

$$\phi'(0) = -\frac{mPr}{1+n\sqrt{Pr}} \tag{31}$$

which gives the proper variation of the surface temperature gradient with Prandtl number at high and low Prandtl numbers. The graph in Fig. 7 shows that the slope of the curve on the logarithmic axes is equal to one for low Prandtl numbers ($Pr < 0.1$) and is equal to 0.5 for high Prandtl numbers ($Pr > 10$). Therefore, for high Prandtl numbers, Eq. (30) is parallel to but slightly below the full similarity solution for $Pr > 10$, while for low Prandtl numbers, Eq. (27) is parallel to but noticeably less than the similarity solution even for $Pr = 0.001$. Therefore, the coefficients, m and n, are not equal to the values predicted by Eqs. (27) and (30). The differences occur because the assumptions concerning the values of $f(\eta)$ and $f'(\eta)$ for low and high Prandtl numbers are not valid near the surface, so that the values of the surface temperature gradient predicted by Eqs. (27) and (30) are accurate qualitatively.

The local Nusselt number given by Eq. (22) can be written for low Prandtl numbers as:

$$Nu_x \approx Ma_x^{1/3}\, Pr^{2/3}\left(\frac{x}{L}\right)^{(k+2)/3}\frac{k+2}{3}f(\infty) \tag{32}$$

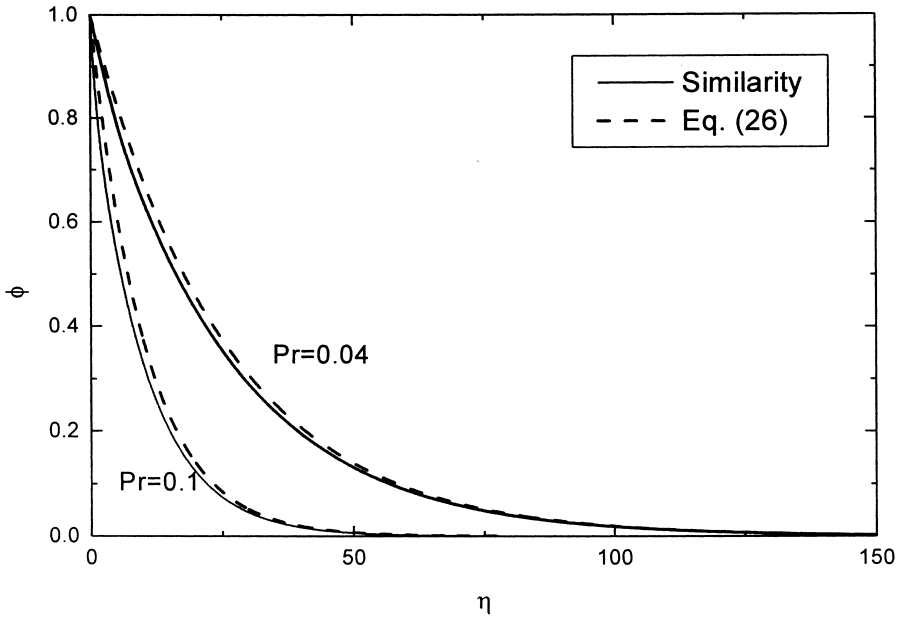

Fig. 5. Temperature distributions for low Prandtl numbers and $k = 0$.

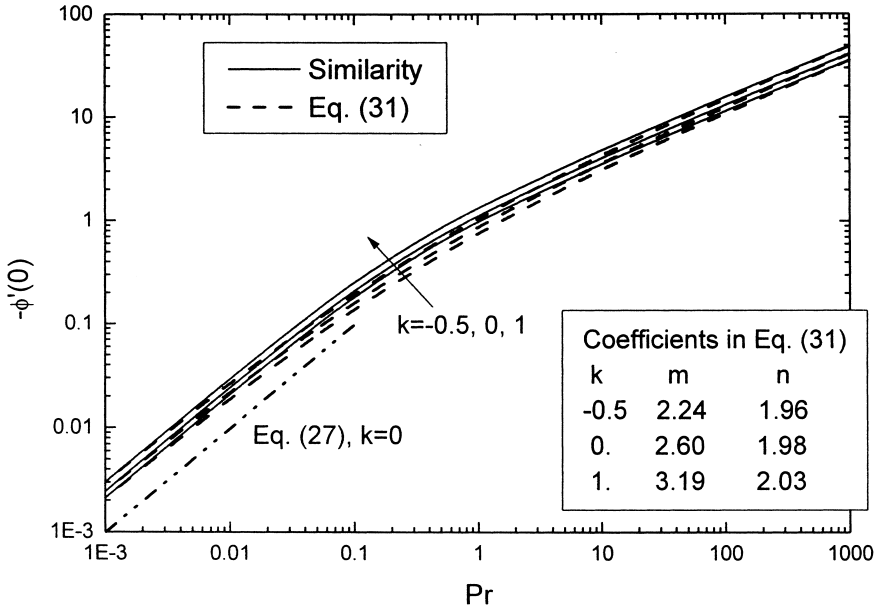

Fig. 6. Effect of surface temperature gradient.

and for high Prandtl numbers:

$$Nu_x \approx Ma_x^{1/3}\, Pr^{1/6}\left(\frac{x}{L}\right)^{(k+2)/3}\sqrt{(k+1)f'(0)} \tag{33}$$

Therefore, the slope of the Nusselt number is proportional to the two-thirds power of the Prandtl number for low Prandtl numbers and is proportional to the one-sixth power of the Prandtl number for high Prandtl numbers, as the thermal boundary layer becomes thinner than the velocity boundary layer. In addition, the coupling of the temperature and flow fields means that the exponent k and the values of $f(\infty)$ and $f'(0)$ are functions of Marangoni and Prandtl

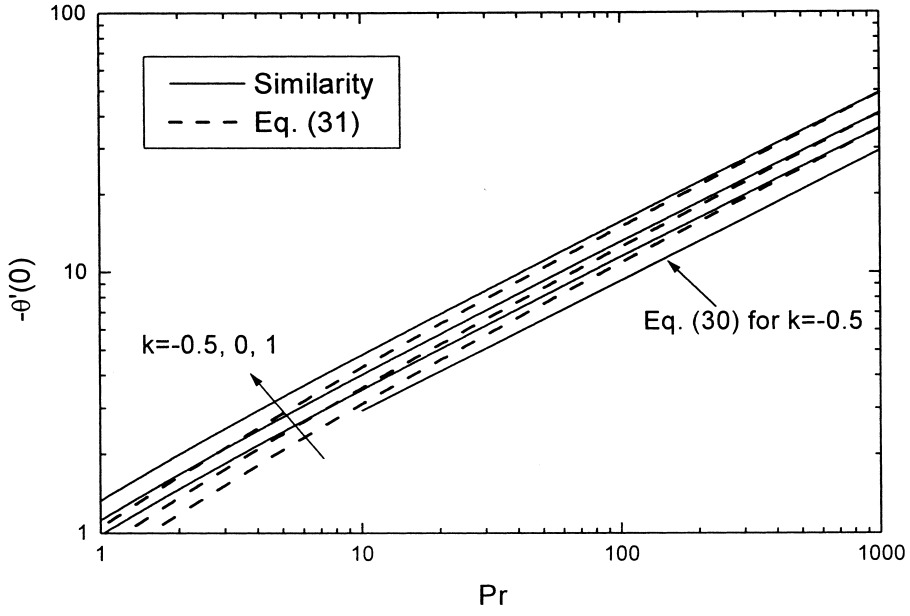

Fig. 7. Surface temperature gradients for $Pr > 1$.

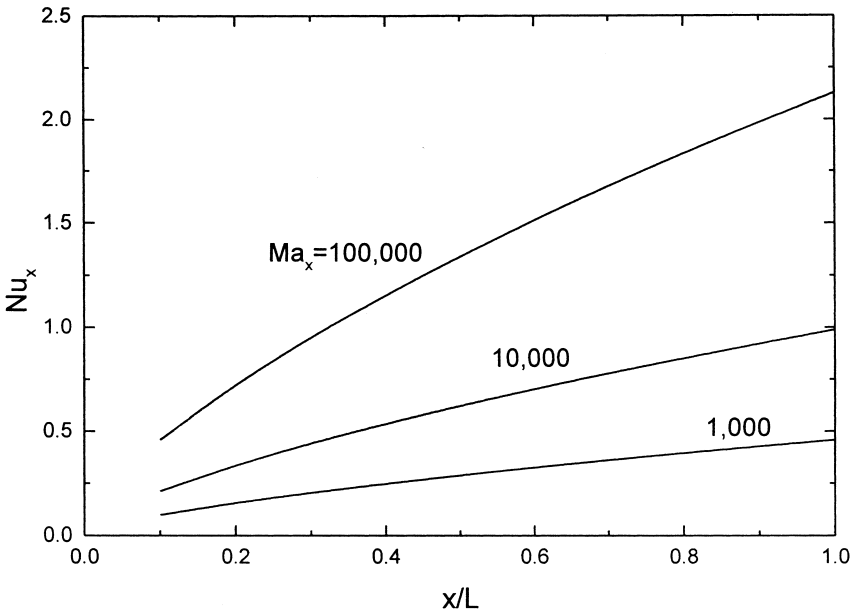

Fig. 8. Predicted local Nusselt number for low Prandtl numbers ($Pr < 0.01$) and $k = 0$.

numbers which will introduce additional Marangoni and Prandtl number effects.

The variation of the local Nusselt number with the Marangoni number and location is shown in Fig. 8 for low Prandtl numbers ($Pr = 0.01$) and in Fig. 9 for high Prandtl numbers ($Pr = 100$). Both graphs are for a linear surface temperature gradient, $k = 0$. The increased flow at higher Marangoni numbers has a significant effect on the heat transfer even for low Prandtl numbers (liquid metals) where conduction is significant.

The average Nusselt number along the surface for

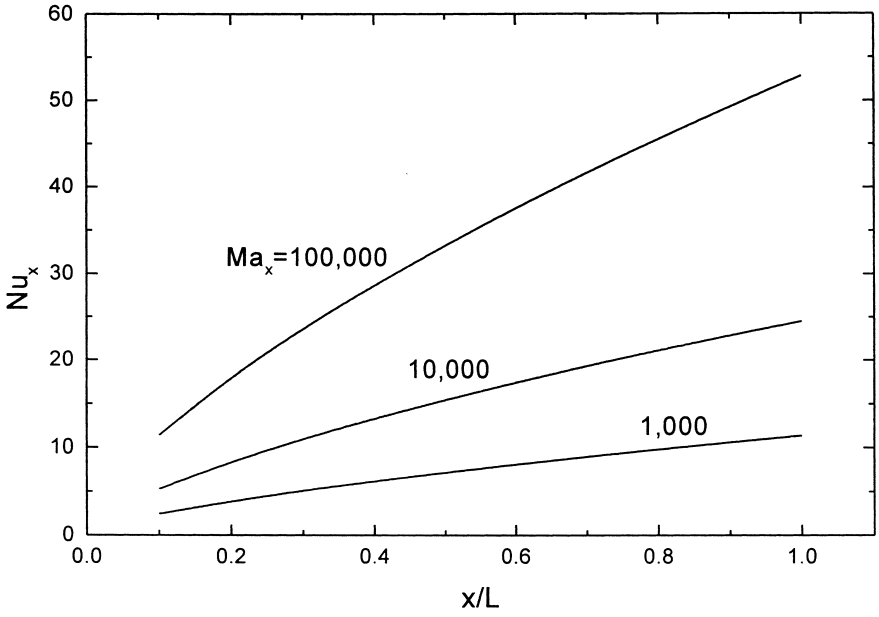

Fig. 9. Predicted local Nusselt number for high Prandtl numbers ($Pr > 100$) and $k = 0$.

low Prandtl numbers using Eq. (27) for the temperature derivative in Eq. (23) is:

$$Nu_L \approx \frac{(k+2)^2}{4k+5} f(\infty) Ma_L^{1/3}\, Pr^{2/3} \tag{34}$$

and for high Prandtl numbers, using Eq. (30) for the temperature derivative in Eq. (23) is:

$$Nu_L \approx \frac{3k+6}{4k+5} \sqrt{(k+1)f'(0)}\, Ma_L^{1/3}\, Pr^{1/6} \tag{35}$$

The predicted average Nusselt number variation with the surface temperature gradient exponent, k, and the Marangoni number is shown in Fig. 10. The figure shows that the Nusselt number is much larger for high Prandtl numbers and that, the exponent k has little effect on the average Nusselt number, especially for high Prandtl numbers. As shown in Fig. 11, the coefficient in Eq. (35), which includes all of the effects due to the exponent k, varies by at most 5% for k from -0.75 to 2. Therefore, for high Prandtl numbers, a reasonable estimate of the average Nusselt number, regardless of the temperature gradient, will be:

$$Nu_L \approx 1.45 Ma_L^{1/3}\, Pr^{1/6} \tag{36}$$

For low Prandtl numbers, the variation of the coefficient in Eq. (34) is much larger, with the value of the coefficient at $k = -0.75$ more than twice the value at $k = 1$.

The thermal boundary layer thickness is defined as usual as the location where the temperature difference is 1% of the total temperature difference, i.e.

$$\phi(\eta_t) = 0.01\, \phi(0) \tag{37}$$

The thermal boundary layer thickness over the entire range of Prandtl numbers is given in Fig. 12. Using Eq. (26) for low Prandtl numbers, the thermal boundary layer thickness can be defined as:

$$\eta_t = \frac{-\ln(0.01)}{Pr\, f(\infty)[(2+k)/3]} \tag{38}$$

while for high Prandtl numbers, using Eq. (29), the thermal boundary layer thickness can be defined as:

$$\eta_t = \frac{-\ln(0.01)}{\sqrt{(1+k)Pr\, f(\infty)}} \tag{39}$$

Eq. (38) is coincident with the lines in Fig. 12 for low Prandtl numbers. Eq. (39) is somewhat higher than the similarity solution, but parallel to it. The discrepancy occurs because the assumptions concerning the values of $f(\eta)$ and $f'(\eta)$ for low and high Prandtl numbers are not valid near the surface, as mentioned before. However, the trends indicated by Eqs. (38) and (39) are correct. The thermal boundary layer thickness variation will be inversely proportional to the Prandtl number for low Prandtl numbers and inversely proportional to the square root of the Prandtl number for high Prandtl numbers. Also, the influence of the exponent k is greater for high Prandtl numbers as shown in Fig. 12. In general, the thermal boundary layer thickness variation can be written as a function of the Prandtl number as:

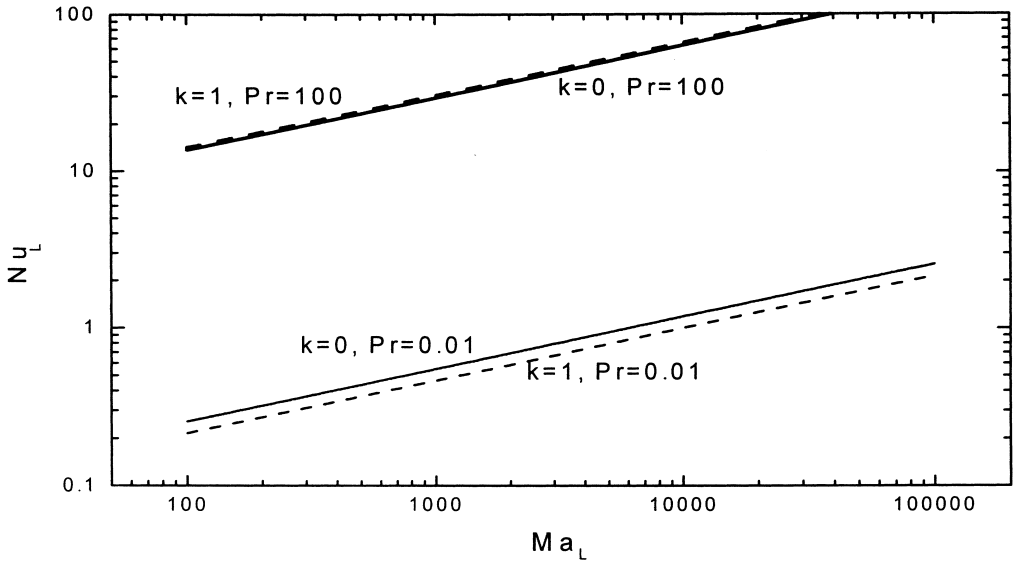

Fig. 10. Predicted average Nusselt numbers for high and low Prandtl numbers.

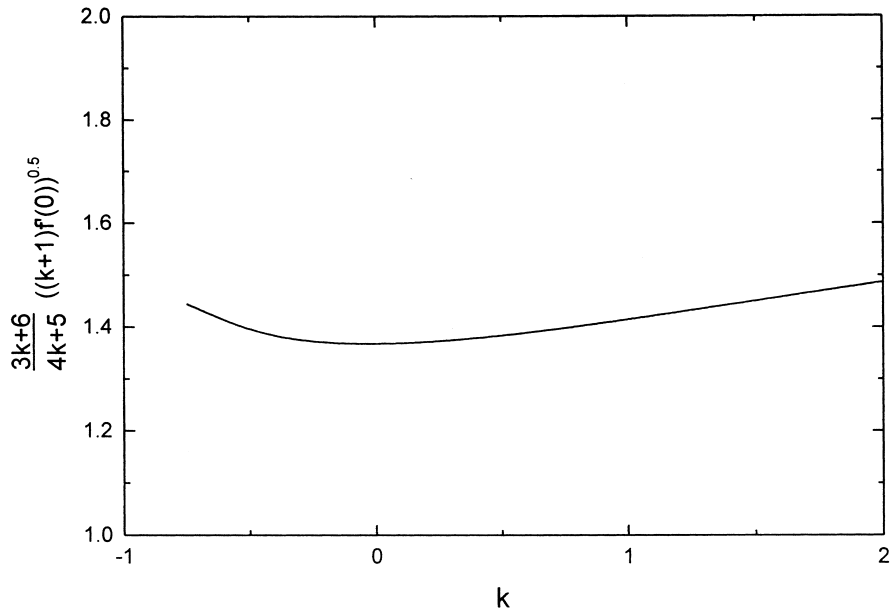

Fig. 11. Predicted coefficient in Eq. (35) to illustrate the effect of temperature gradient.

$$\eta_t = \frac{1 + m_\delta \sqrt{Pr}}{n_\delta \, Pr} \tag{40}$$

Eq. (40) is plotted in Fig. 12 for $k = 0$. The values of n_δ agree well with Eq. (38) while the values of m_δ/n_δ are somewhat smaller than the corresponding coefficient in Eq. (39).

The similarity analysis, based on the boundary layer equations, assumes that the transverse derivatives of the velocity and temperature are much larger than

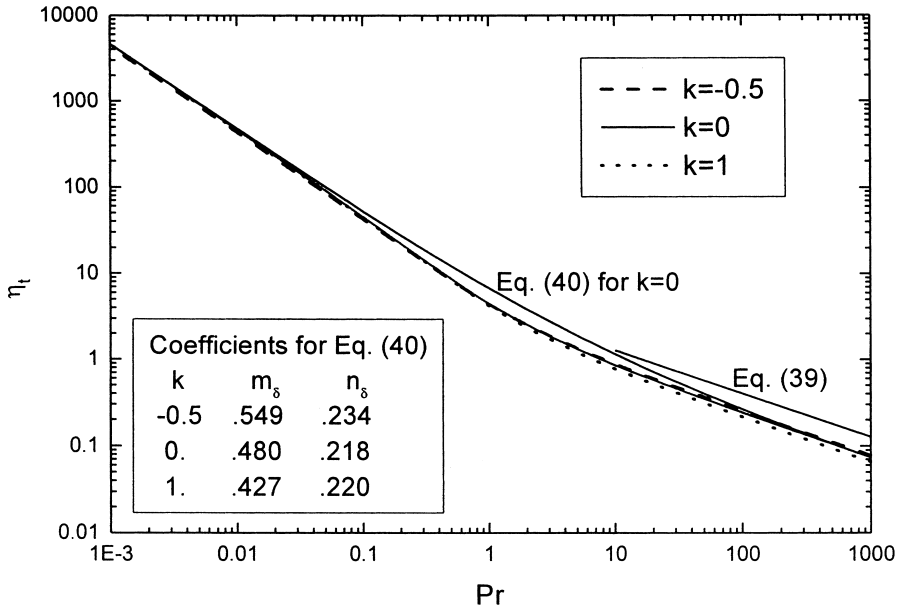

Fig. 12. Predicted thermal boundary layer thickness for various conditions.

their axial derivatives. Analysis of the similarity transformation shows that both are true if:

$$C_1 L^{(k+2)/3} = \sqrt[3]{\frac{(\mathrm{d}\sigma/\mathrm{d}T)A\rho L^{k+2}}{\mu^2}} = Ma_L^{1/3}\, Pr^{-1/3} \gg 1 \tag{41}$$

4. Conclusions

Marangoni convection has been analyzed for boundary layer flow over a flat surface with an imposed temperature gradient. The governing equations were solved using a similarity analysis applicable to both linear and non-linear temperature gradients. For a liquid pool heated at both ends, the surface temperature gradient would only be expected to be linear for low Prandtl number fluids where the conduction in the fluid is much greater than the convection heat transfer. The predicted surface velocities agree well with the measured values for a shallow pool of liquid indium [8].

The analysis gives the variation of the velocity and temperature distributions in the boundary layer for power-law variations of the surface temperature gradient. Equations are given for the surface velocity, the total mass flow rate and the heat flux at the interface as functions of Marangoni, Prandtl and Reynolds numbers, the temperature gradient exponent k and the location. For $k = 0$, the analysis agrees with previous results for a linear temperature gradient (Okano et al. [6]) that the Reynolds number based on the surface velocity varies as the two-thirds power of the Marangoni number. The solution of the simplified governing equations shows that the Nusselt number is proportional to the two-thirds power of the Prandtl number for low Prandtl numbers ($Pr < 0.1$) and is proportional to the one-sixth power of the Prandtl number for high Prandtl numbers ($Pr > 10$) as the thermal boundary layer becomes thinner than the velocity boundary layer. The analysis also shows that for high Prandtl numbers, the average Nusselt number is practically independent of the surface temperature gradient, so Eq. (35) can be used in general for high Prandtl numbers.

For normal boiling of water, the Marangoni convection boundary layer around a vapor bubble predicted by this analysis would be much less than the expected bubble radius, so the present results can be used as an initial estimate of the effect of Marangoni induced flow around a vapor bubble.

Acknowledgements

The project was financially supported by the National Natural Science Foundation of China with grant number 59995550-3.

References

[1] J. Straub, The role of surface tension for two-phase heat and mass transfer in the absence of gravity, Exp. Thermal Fluid Sci. 9 (1994) 253–273.
[2] D.M. Christopher, B.X. Wang, Marangoni convection around a bubble in microgravity, heat transfer, in: Proceedings of the 11th International Heat Transfer Conference, 3, Taylor and Francis, Levittown, PA, 1998, pp. 489–494.
[3] A. Eyer, H. Leist, R. Nitsche, Floating zone growth of silicon under microgravity in a sounding rocket, J. Crystal Growth 71 (1985) 173–182.
[4] K. Arafune, A. Hirata, Interactive solutal and thermal Marangoni convection in a rectangular open boat, Numerical Heat Transfer Part A 34 (1998) 421–429.
[5] A. Croll, W. Muller-Sebert, R. Nitsche, The critical Marangoni number for the onset of time-dependent convection in silicon, Mater. Res. Bull. 24 (1989) 995–1004.
[6] Y. Okano, M. Itoh, A. Hirata, Natural and marangoni convections in a two-dimensional rectangular open boat, J. Chem. Eng. Jpn. 22 (1989) 275–281.
[7] K. Arafune, M. Sugiura, A. Hirata, Investigation of thermal Marangoni convection in low and high Prandtl number fluids, J. Chem. Eng. Jpn. 32 (1999) 104–109.
[8] K. Arafune, A. Hirata, Thermal and solutal Marangoni convection in In–Ga–Sb system, J. Crystal Growth 197 (1999) 811–817.
[9] S. Slavtchev, S. Miladinova, Thermocapillary flow in a liquid layer at minimum in surface tension, Acta Mech. 127 (1998) 209–224.
[10] D. Schwabe, J. Metzger, Coupling and separation of buoyant and thermocapillary convection, J. Crystal Growth 97 (1989) 23–33.